Volume 14
Number 42
14 November 2023
Pages 4777-4870

Polymer Chemistry

rsc.li/polymers

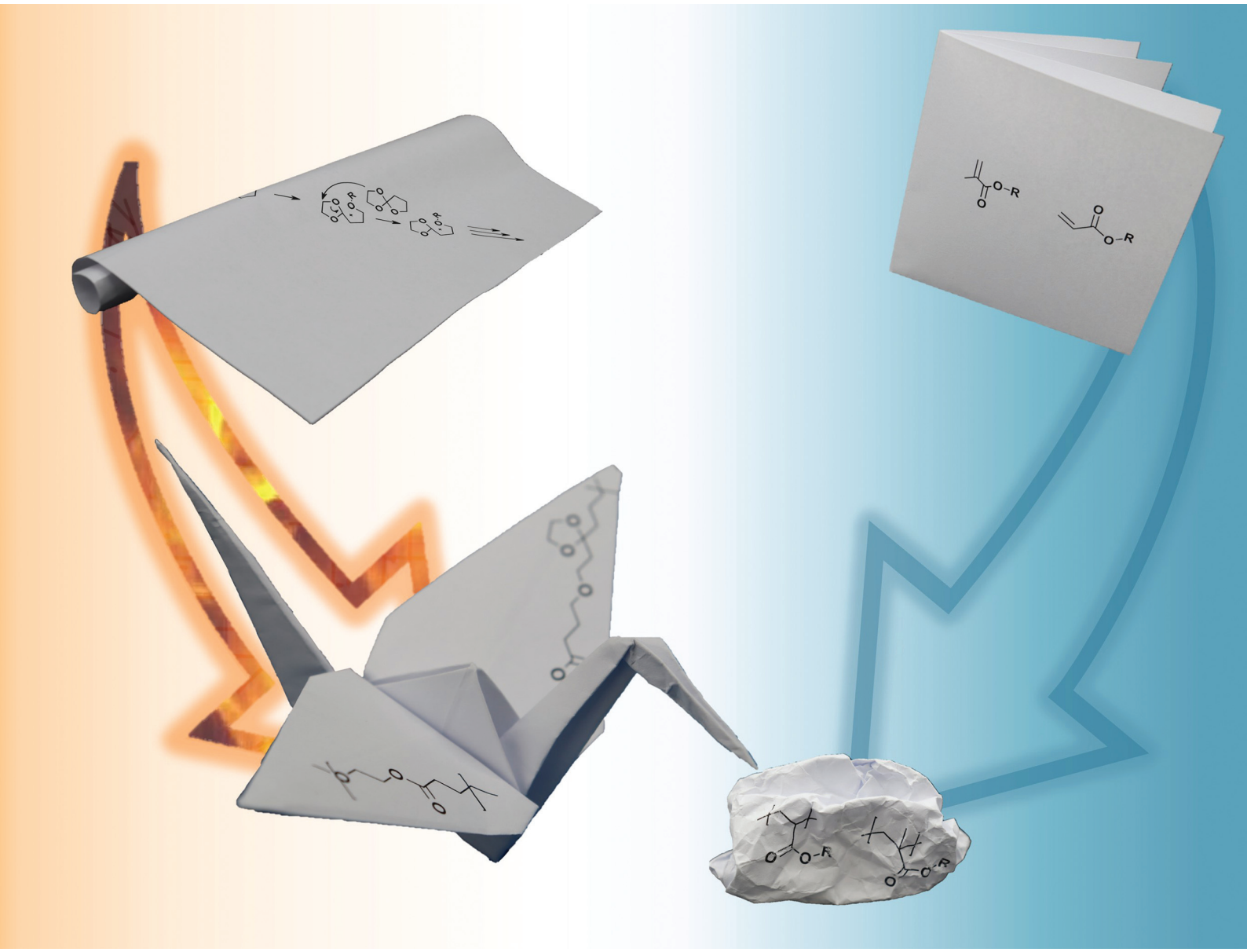

ISSN 1759-9962

ROYAL SOCIETY OF CHEMISTRY

PAPER

Katharina Ehrmann *et al.*
Stereolithographic 3D printing of pure poly(ether–ester) networks from spirocyclic monomers *via* cationic ring-opening photopolymerization at high temperatures

Polymer Chemistry

ROYAL SOCIETY OF CHEMISTRY

PAPER

View Article Online
View Journal | View Issue

Cite this: *Polym. Chem.*, 2023, **14**, 4809

Stereolithographic 3D printing of pure poly(ether–ester) networks from spirocyclic monomers *via* cationic ring-opening photopolymerization at high temperatures†

Danijela Kojic,[a,b] Katharina Ehrmann, *[a] Raffael Wolff,[a] Yazgan Mete,[a] Thomas Koch,[c] Jürgen Stampfl, [b,c] Stefan Baudis [a,b] and Robert Liska [a]

Received 3rd July 2023,
Accepted 12th September 2023

DOI: 10.1039/d3py00787a

rsc.li/polymers

We demonstrate for the first time stereolithographic (SL) printing of pure poly(ether–esters) based on cationic ring-opening photopolymerization without the need to accelerate curing *via* radical mechanisms. To minimize shrinkage stress in bulk-photopolymer parts, spiro-orthoesters have been utilized as expanding monomers. In combination with a bifunctional spiro-orthoester or epoxide, previously inaccessible pure aliphatic poly(ether–ester) parts have been printed *via* Hot Lithography, an SL process at elevated temperatures. Precision part size, high resolution and excellent surface-finish could be achieved. During monomer evaluation, the changes in reactivity and polymerization mode of photopolymerization at elevated temperatures were investigated with photo-DSC analysis. Convincing (thermo-)mechanical properties of the cured materials were determined with DMTA and tensile testing. This technological advance gives access to SL manufacturing of a highly regarded material class due to the biocompatibility and biodegradability of aliphatic poly(ether–esters), which frequently find application in medical applications where flexible and highly precise part design is key.

Introduction

Additive manufacturing (AM), also known as 3D printing or rapid prototyping, was invented in the early 1980s and quickly developed into a significant polymer processing method.[1] Within this field, stereolithography (SL) is a well-known method utilizing, *e.g.*, a laser to cure liquid photopolymerizable monomers in a spatially resolved manner point by point and layer by layer to produce three-dimensional parts with outstanding precision.[2] Recently, this technique has been developed further into the Hot Lithography process to accommodate the necessity of heating the photopolymerization process during manufacturing.[3,4]

Conventional monomers used for SL are acrylates and methacrylates due to their high reactivities at room temperature and good hardness of resulting networks.[5] However, these monomers and thereof produced parts may cause adverse health effects and are generally non-degradable.[1] From a manufacturing point of view they suffer from high polymerization shrinkage during the solidification of liquid resin (Fig. 1A).[6] This significantly reduces surface properties and may lead to deformation and crack formation in produced parts.[1,2] Therefore, use of expanding monomers, from which intrinsically biocompatible and biodegradable materials are produced during SL printing, would be beneficial.

In this context, spiro-orthoesters could provide a biocompatible, biodegradable alternative since their cationic ring-opening polymerization (ROP) leads to pure aliphatic poly(ether–esters). For example, the aliphatic poly(ether–ester) polydioxanone obtained by ring-opening polymerization of *p*-dioxanone and is widely used in the biomedical sector as suture material (PDS™) due to its good biodegradability and biocompatibility.[7,8] Additionally, aromatic poly(ether–esters) comprised of poly(ethylene glycol) and poly(butyleneterephtalate) segments (PolyActive®) are intensively studied as bone replacement and artificial skin materials.[9] *In vivo* degradation is

[a]*Institute of Applied Synthetic Chemistry, Technische Universität Wien, Vienna, Austria. E-mail: katharina.ehrmann@tuwien.ac.at*
[b]*Christian Doppler Laboratory for Advanced Polymers for Biomaterials and 3D Printing, Institute of Applied Synthetic Chemistry, Technische Universität Wien, Vienna, Austria*
[c]*Institute of Materials Science and Technology, Technische Universität Wien, Vienna, Austria*

† Electronic supplementary information (ESI) available Experimental procedures, monomer reactivity and polymerization mode study, additional network characterization. See DOI: https://doi.org/10.1039/d3py00787a

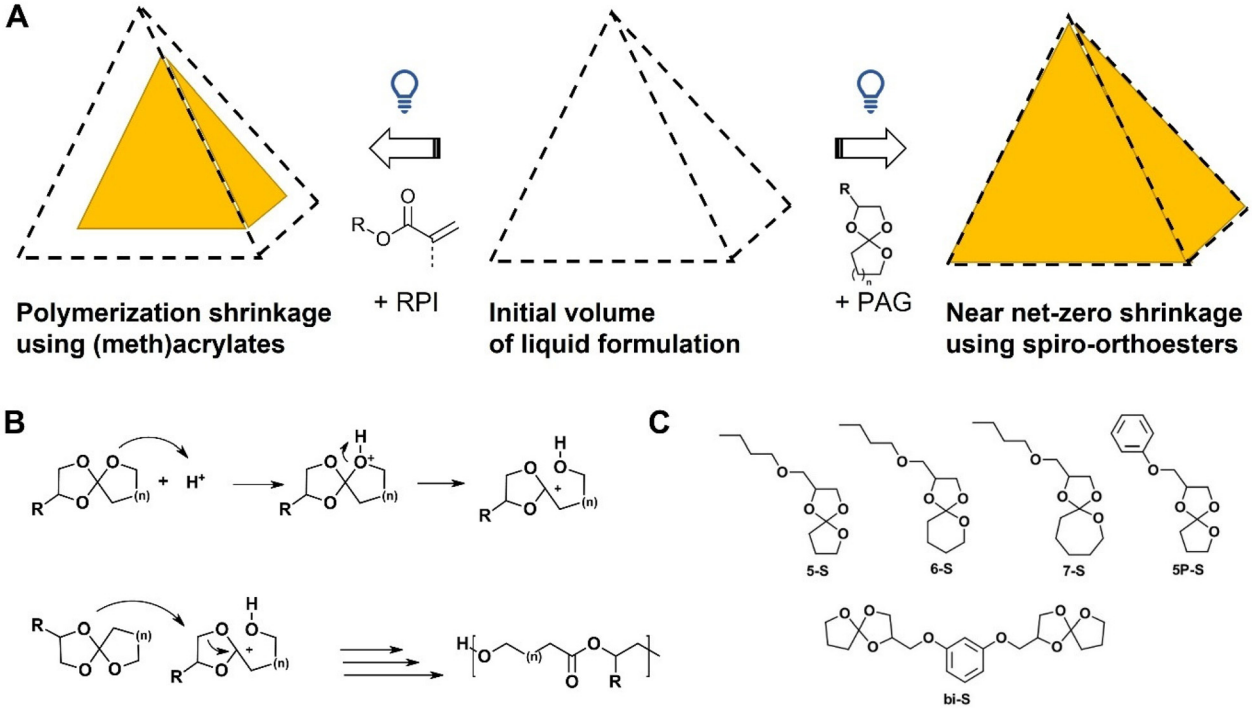

Fig. 1 Schematic representation of shrinkage behavior of conventional (meth)acrylates and ring-opening monomers such as spiro-orthoesters during photopolymerization initiated by radical initiators (RPI) and photo acid generators (PAG), respectively (A) and employed single (top) and double (bottom) ring-opening polymerization mechanisms of spiro-orthoesters (B) for the photopolymerization of mono- (top) and difunctional (bottom) spiro-orthoester monomers explored in this work (C).

enabled through hydrolysis of ester bonds and a phagocyte-derived oxidative degradation of the polyethers.[9]

Beside these advantages, the monomer class of spiro-orthoesters has also been found to significantly reduce volumetric shrinkage.[10–13] Its polymerization is strongly temperature-dependent, where single ring-opening (SRO, Fig. 1B, top) already occurs at room temperature. Under optimal polymerization conditions the initially formed poly(cyclic-orthoester) isomerizes into a poly(ether–ester) in a process known as double ring-opening (DRO, Fig. 1B, bottom).[12–15] While some studies report ROP of spiro-orthoesters at elevated temperatures, the effects of temperature on polymerization behavior with respect to SRO/DRO ratio and side reactions has never been studied systematically. However, this will of course impact the final volumetric change from liquid formulation to cured polymer.

The first light-initiated cationic ROP, where a super acid was released from a photo acid generator by irradiation to initiate polymerization of a mixture of spiro-orthoester and epoxide monomers, was described in 1984.[16] The photopolymerization of a cycloaliphatic five-membered spiro-orthoester with accompanying side-reactions was reported by Hsu and Wan.[17] Nowadays, spiro-orthoesters are widely used as anti-shrinkage additives in commercial polymerizations.[13] These studies of pure cationic ROP were all conducted at room temperature and report long polymerization times, which are unsuitable for SL printing. Marx *et al.* utilized parallel cationic ROP of spiro-orthoesters as shrinkage-controlling agents and radical thiol–ene photopolymerization to obtain printable formulations with volumetric expansions up to 1.7%.[18] However, up to date, printing of pure poly(ether–esters) *via* photoinitiated cationic ROP could not be achieved.

Herein, we compare photopolymerization behavior and polymerization modes of several spiro-orthoesters in pure cationic ROP between room temperature and 110 °C to determine optimal candidates for printing (Fig. 1C). For the network formation we investigated a bifunctional aromatic spiro-orthoester and a commercial bifunctional epoxide as potential crosslinkers. The resulting materials were characterized thermomechanically and the optimal formulation was printed in a Hot Lithography process.

Results and discussion

Monomer synthesis

Spiro-orthoester monomers with varying ring-sizes (n = 1–3, Fig. 1) were synthesized (Fig. 1C, for details refer to ESI†) to investigate their photoreactivity since the Gibbs free energy of polymerization, and thus the occurrence of the polymerization reaction, depends on the ring strain energy of the monomers.[19,20] Furthermore, the rings were substituted with an aliphatic ether motif and an aromatic motif, which may have an impact on monomer reactivity and material properties of the derived polymers. The monofunctional monomers were

synthesized from the corresponding commercially available lactones and epoxides.[21,22]

A rigid, bifunctional spiro-orthoester was also synthesized as a crosslinker (see ESI†). More reactive epoxide-based crosslinkers can also be utilized to obtain pure poly(ether–esters) as products. These are usually derived from bisphenol A diglycidylether (BADGE).[23] However, the melting points of such monomers are above the maximum operating temperatures of the Hot Lithography device (120 °C). Therefore, we synthesized a spiro-orthoester crosslinker based on resorcinol diglycidyl ether, which introduces more flexibility to the monomer[23] and as a result the melting point was successfully lowered to 105 °C, which is within the accessible temperature range.

Table 1 Results obtained from the photoreactivity study of spiro-orthoesters (S) of different ring sizes and structures (5–7; butyl or phenyl (P) substituent) at 110 °C initiated by 1 mol% tBuI-Al: number average molecular weight ($\overline{M_n}$), molecular weight distribution ($Đ$), degree of polymerization (P_n), conversion (C)

Monomer	M_n [a] [Da]	$Đ$ [a] [–]	P_n [b] [–]	C [c] [%]
5-S	560	1.74	3	61
6-S	2 400	1.35	10	14
7-S	1 500	1.25	6	65
5P-S	490	1.08	2	94

[a] Determined with SEC analysis utilizing conventional calibration. [b] Calculated from $\overline{M_n}$. [c] Determined with NMR-analysis.

Reactivity study

Influence of ring size and substitution. In general, cationic ring-opening photopolymerization is initiated by photoacids generated upon photolysis of so-called photoacid generators (PAGs).[24,25] Onium salts, consisting of a positively charged cation bound to aromatic rings (*e.g.* sulfur and iodine) and a counter anion are the most commonly used PAGs in literature.[25,26] Thus, the highly reactive diphenyliodonium salt tBuI-Al was used as the PAG for the cationic photopolymerization of the synthesized spiro-orthoesters. While the reactivity study was conducted at temperatures from 25 °C to 110 °C (Table S1†), comparison of effects of monomer ring size and substitution on polymerization behavior was conducted at 110 °C (Table 1). Reactivity is often assessed *via* the heat of polymerization. However, low and poorly detectable

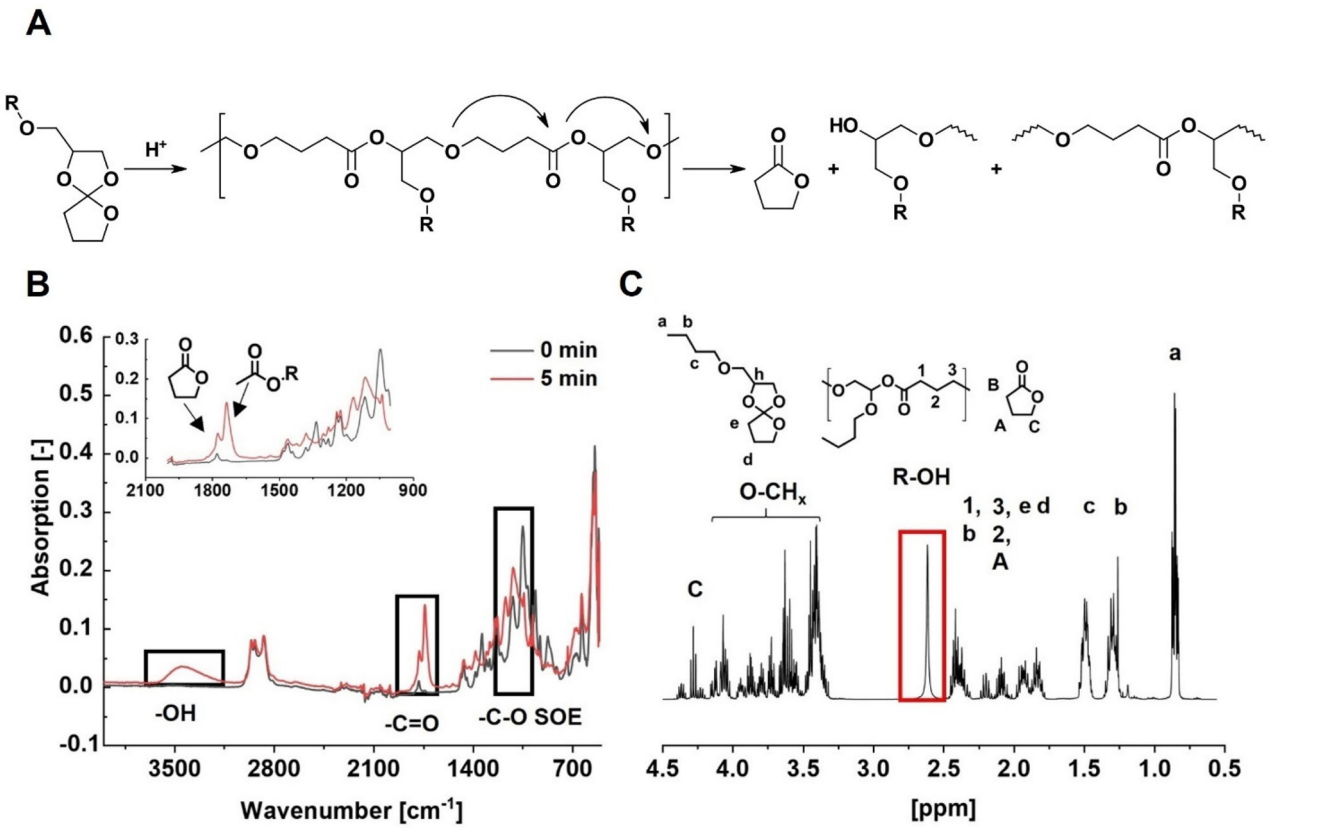

Fig. 2 Depolymerization reaction of poly(ether–esters) *via* backbiting as observed for 5-S and 5P-S (A). Corresponding ATR-IR spectra of 5-S before (0 min) and after photopolymerization (5 min) evidence formation of carbonyl-groups due to polymerization of spiro-orthoesters and formation of γ-butyrolactone due to depolymerization (B). ^{1}H-NMR (400 MHz, $CDCl_3$) spectra after the photopolymerization of 5-S confirming the formation of γ-butyrolactone and new hydroxyl-groups (C).

polymerization enthalpies are expected for spiro-orthoesters due to the generally low ring strain energy of the monomers, which is the driving-force for ring-opening polymerizations.[27,28] Indeed, exothermic behavior of the investigated spiro-orthoesters was too low to detect during photo-DSC and meaningful calorimetric data could not be collected, even at 110 °C. Nevertheless, photopolymerization with the photo-DSC setup is highly advantageous, as it offers inert atmosphere with reproducible conditions and requires only small amounts of the formulation. This controlled irradiation process conducted at different temperatures provides an excellent basis for subsequent studies *via* NMR and SEC to provide information about the monomer conversion and the molecular weight of the polymers.

Monomer conversions of 5-S and 7-S are quite similar while the aromatic 5P-S reaches the highest monomer conversion of 94%. 6-S is the least reactive monomer with a conversion of only 14%. These results agree with theoretical calculations predicting the reactivity of monomers of different ring-sizes.[28] The low reactivity of six-membered rings is caused by their favourable geometry.

The molecular weights of the resulting polymers follow a different trend than expected from monomer reactivity. 6-S and 7-S result in higher molecular weights compared to the five-membered 5-S and 5P-S due to the occurrence of the backbiting-reaction for five-membered rings (Fig. 2A). During this side reaction, γ-butyrolactone and low molecular weight oligomers with hydroxyl groups are formed, which was confirmed for both five-membered spiro-orthoesters with ATR-IR and NMR-analysis (Fig. 2C and D, respectively). The formation of the lactone band at 1170 cm^{-1} after photopolymerization is clearly visible. Furthermore, lactone-specific NMR-signals as well as a distinct broad singlet, which is indicative of an OH-group, were found.

Influence of temperature. As mentioned previously, SRO and DRO during cationic ROP of spiro-orthoesters is a temperature-dependent process.[12,15] The probability for DRO is known to increase with increasing temperature.[12,29] Thus, the resulting polymer does not consist of one structure entirely but is a mixture of poly(cyclic-orthoesters) and poly(ether–esters).[12] For cationic photopolymerization specifically, previous mechanistic investigations of cycloaliphatic spiro-orthoesters have shown monomer-dependent behaviour regarding side reactions occurring during SRO and regiospecific DRO.[17,30–32] Therefore, we conducted a temperature-dependent mechanistic study to find the optimum temperature range for bulk photopolymerization of the synthesized monomers as an indicator for otimal printing conditions during SL printing. Photopolymerizations of the spiro-orthoester monomers were conducted at 25, 70, 90, and 110 °C (Table S1†). The dependence of the photopolymerization process on temperature was clearly visible in the increase in monomer conversion and molecular weights of the polymers and decrease of the SRO/DRO ratio with temperature (Fig. 3). To understand the differences between the individual monomers, their affinity for side-reactions as well as different polymerization modes must be considered. NMR analysis of the products gave reliable indications about conversion, the severeness of backbiting side reactions, and to which extent SRO or DRO occurred (for detailed analysis refer to ESI†). With increasing temperature, monomer conversions increased, which is untypical for equilibrium ring-opening reactions of small ring monomers. Comparing the occurrence of the equilibrium SRO with irreversible DRO with increasing temperature, DRO was overproportionally increased for all analyzed spiro-orthoesters, effectively trapping the polymerized state opposed to the depolymerized state. 5-S and 7-S reach very similar monomer conversions above 70 °C. The conversion

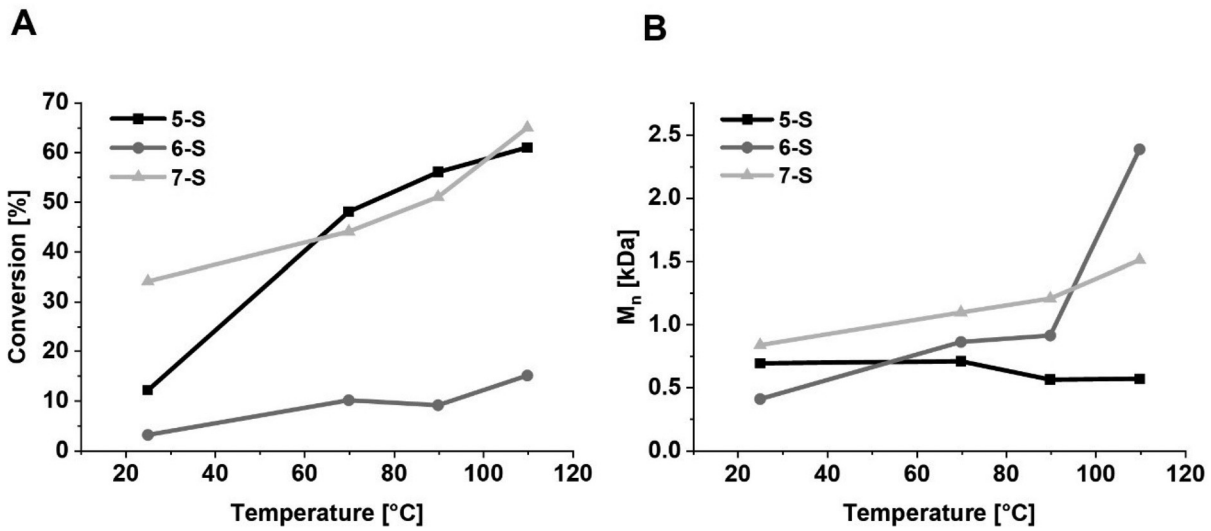

Fig. 3 Polymerization temperature dependence of monomer conversion (A) and molecular weight (B) of resulting polymers derived from cationic ROP of aliphatically substituted spiro-orthoesters (S) of different ring sizes (5–7), initiated by 1 mol% tBuI-Al.

of less reactive 6-S also increases with temperature but still only reaches a modest conversion of 14% at 110 °C. As discussed previously, this behaviour is linked to the ring size of the cyclic ether ring. The stable conformation of the six-membered 6-S leads to a low ring strain and subsequently to inherently low reactivity.

The molecular weight of the polymers increases moderately with temperature for 6-S and 7-S due to enhanced polymerization compared to back-biting. On the contrary, the molecular weight of 5-S decreases slightly with increasing temperature. This is because depolymerization of the formed poly(ether–ester), which is favoured at higher temperatures, is much more pronounced for 5-S than for 6-S and 7-S. As already mentioned, the depolymerization process leads to the formation of γ-butyrolactone, which was detected during NMR analysis. With the obtained detailed knowledge about the polymerization modes and reactivities an informed decision on which monomers are most suitable for network formation was possible. During photopolymerization of 5-S and 7-S, SRO and DRO took place simultaneously in the investigated temperature range (Schemes S1 and S3†). Thus, both monomers are promising candidates for bulk-photopolymerizations. Higher temperatures led to better conversion and are therefore favourable for swift bulk polymerization required for SL printing. 6-S only polymerized sluggishly *via* SRO at all temperatures (Scheme S2†) and was therefore excluded as potential monomer.

Network formation studies

To obtain photopolymer networks, two crosslinking strategies were examined: the bifunctional spiro-orthoester bi-S could be utilized at temperatures above 110 °C, where dissolving of solid bi-S up to 65 wt% in the monofunctional monomer was possible. Additionally, a traditional bifunctional epoxide was employed as crosslinker, which also leads to formation of pure poly(ether–esters).

Crosslinking with bifunctional spiro-orthoester. The synthesis and purification of a five-membered bifunctional spiro-orthoester was considered more straightforward than that of the seven-membered difunctional compound based on the synthesis experiences for monofunctional spiro-orthoesters. Thus, a five-membered bifunctional spiro-orthoester bi-S was synthesized (Fig. S5†) and used as crosslinker in bulk polymerizations with monofunctional spiro-orthoesters to examine a purely spiro-orthoester-based formulation (Fig. S16†). To ensure a uniform system in terms of reactivity and polymerization mechanism, five-membered monofunctional monomers were chosen for the network formation. Hence, the aromatic 5P-S and the aliphatic 5-S were polymerized with the bifunctional monomer to determine the influence of the substituents on the mechanical properties of the network. For optimization of the network, crosslinker contents were varied between 25 and 65 wt%. Bulk polymerization of purely spiro-orthoester-based formulations at 120 °C led to viscous but not form-stable specimens within printing-appropriate time frames due to their moderate reactivity. The samples only became solid after additional thermal postcuring at 120 °C. In the case of 5-S, this post-curing process resulted in thin final specimens due to the monomer's volatility during prolonged heat exposure (>1 h).

The aliphatic poly(ether–esters) obtained purely from spiro-orthoesters were tested (thermo)mechanically (Fig. S17–S22, Tables S2 and S3†). A positive influence of the aromatic monomer 5P-S on the thermomechanical properties was observed (Fig. S20–22†). While the glass transition temperature could be increased successfully compared to the materials comprised of the aliphatic monomer 5-S (Table S4†), the T_g was still quite low at 23 °C. The (thermo-)mechanical properties of pure spiro-orthoester-based networks varied with crosslinker content but could generally achieve remarkable tensile toughness of 7.6 MJ m^{-3} at the optimal composition (Fig. S20, Table S5†). However, the onset of elongation occurred already at low loadings indicating a more rubbery than plastic deformation behaviour. Therefore, the pure spiro-orthoester systems were rendered unsuitable for Hot Lithography.

Crosslinking with bifunctional epoxide. To optimize the final (thermo)mechanical performance and enhance reactivity of the spiro-orthoester-based system, a bifunctional epoxide was employed as crosslinker as it still produces degradable poly(ether–esters) with decreased polymerization shrinkage (Fig. S6A†).[33,34] Thus, the commercially available epoxide 3,4-(epoxycyclohexane)methyl-3,4-epoxycyclohexylcarboxylate (CE) was used in combination with the monofunctional aromatic spiro-orthoester 5P-S, which had led to better mechanical network properties than 5-S in the pure spiro-orthoester materials. For comparability with the pure system, the same crosslinker concentrations were chosen.

The reactivity towards photopolymerization of the epoxide containing system was tested with photo-DSC analysis (Fig. 4A and Table 2). We observed a clear trend between the epoxide content and the reactivity of the system. Importantly, form stability directly after light exposure was achieved for photopolymerization of these formulations at 110 °C.

Predictably, the polymerization enthalpy increased with increasing epoxide content. The formulation with 65 wt% epoxide gave the lowest time until maximum reactivity (t_{max}) and time until 95% conversion (t_{95}) values and highest conversion. The conversion of the bifunctional epoxide CE was determined to be approximately 80% (eqn SII, ESI†).

The incorporation of the spiro-orthoester into the network was confirmed by ATR-IR analysis (Fig. S23 and S24†). The ring-opening polymerization of the spiro-orthoester 5P-S was detected through the decrease in strength of the C–O stretching band at ~1070 cm^{-1}. Additionally, the increase in intensity of the carbonyl band at ~1730 cm^{-1} and the formation of a new OH-band confirm occurrence of ROP.

The viscoelastic behaviour of the resulting poly(ether–esters) was investigated with dynamic mechanical thermal

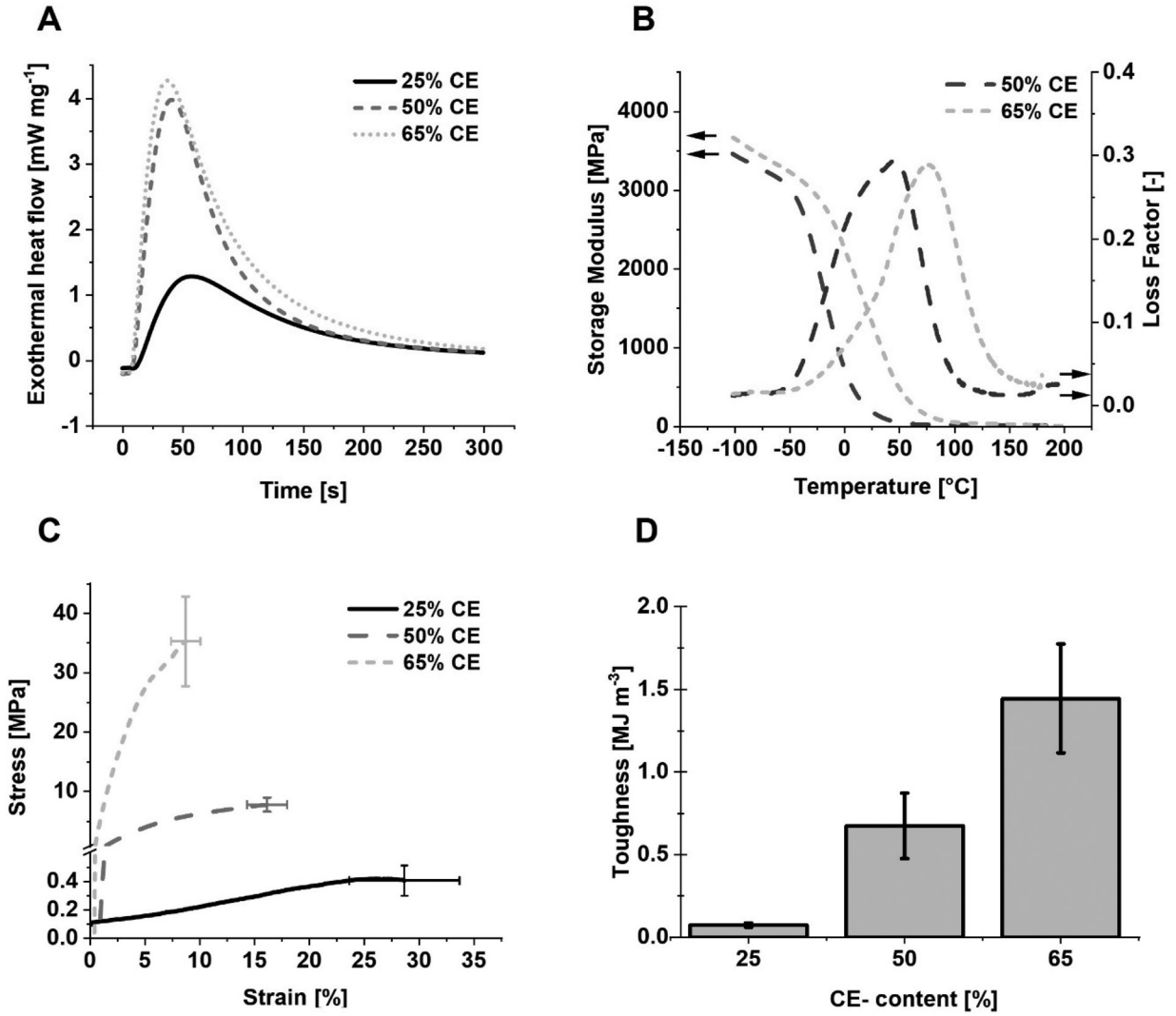

Fig. 4 Photo-DSC results for the formulations containing aromatic monofunctional 5P-S and bifunctional epoxide CE in varying concentrations at 110 °C and with 1 wt% IC 290 as photoinitiator (A), storage moduli G' and loss factors tan δ (B), representative tensile testing curves and mean stress and strain at break values (C) and toughness (D) of specimens obtained from the same formulations at 110 °C.

Table 2 Results obtained from the photo-DSC measurements for the systems containing the epoxide CE and 5P-S as monomers in varying compositions (m(CE)) and 1 mol% IC 290 as photoinitiator at 110 °C: time at maximum heat development t_{max}, time at 95% of heat development t_{95}, peak maximum height h, peak area A, conversion C

m(CE) [wt%]	$t_{max.}$[a] [s]	t_{95}[a] [s]	h[a] [mW mg^{-1}]	A[a] [J g^{-1}]	C[b] [%]
25	50 ± 12	200 ± 12	1.5 ± 0.4	140 ± 21	88
50	42 ± 1	180 ± 0	3.8 ± 0.1	283 ± 4	89
65	38 ± 1	187 ± 2	4.1 ± 0.1	337 ± 5	81

[a] Determined with photo-DSC analysis. [b] Determined *via* eqn SIII,† using photo-DSC data.

analysis (DMTA, Fig. 4B). The storage and loss moduli were continuously recorded as a function of temperature and the loss factor (tan δ) was determined. The glass-transition temperature (T_g) was determined as the maximum value of the tan δ curve.

The formulation containing 25 wt% epoxide resulted in a soft material due to the low crosslinking density. Thus, DMTA measurement of these specimens was not possible as they repeatedly failed before reaching the T_g. Materials obtained from formulations containing 50 and 65 wt% epoxide CE exhibited much better mechanical properties and DMTA could be performed successfully. The T_g was increased to 55–77 °C. At 20 °C, materials containing 50 wt% epoxide reach a storage modulus of 240 MPa, whereas those with 65 wt% epoxide content reach 1500 MPa (Fig. 4B, Table S6†). The molecular weight between crosslinks decreased with increasing crosslinker content.

During tensile testing, the materials are exposed to axial tension until failure, which gives a good indication for applicability of developed materials. Therefore, tensile tests were per-

formed with the obtained specimens of both, the spiro-orthoester-crosslinked specimens (Tables S3 and S5†) and the epoxide-crosslinked specimens (Fig. 4C and D). A clear trend between the crosslinker content and the tensile behavior was observed (Table S7†). Low amounts of epoxide result in stretchable and soft materials and consequently high strains at break due to the low crosslinking density. With increasing amounts of the epoxide, stress at break increases and strain at break decreases. Hence, the specimens containing 65 wt% epoxide withstand a mechanical stress of approximately 24 MPa. The strain decrease, however, is disproportionally lower leading to enhanced tensile toughness. According to these results the epoxide significantly improves the thermomechanical properties of the materials compared to the spiro-orthoester crosslinker bi-S while maintaining the chemical identity of pure aliphatic poly(ether–esters) and low shrinkage behavior. This finding is likely directly correlated to the higher conversions found for the epoxide-containing systems, as the increase in mechanical performance was a function of the increase in crosslinker content.

Shrinkage behaviour analysis

To assess the impact of ring-opening spiro-orthoester monomers on shrinkage behaviour of the crosslinked materials, their volume change was determined for the specimens crosslinked with the difunctional spiro-orthoester bi-S as well as for the specimens crosslinked with the epoxide crosslinker CE. Density analysis of the liquid formulations ($\rho_{monomer}$) and corresponding cured specimens ($\rho_{polymer}$) revealed that the volume change (ΔV) according to eqn (1) decreased with increasing spiro-orthoester content in both cases confirming the initial hypothesis.

$$\Delta V(\%) = \left(\frac{\rho_{polymer} - \rho_{monomer}}{\rho_{polymer}}\right) \times 100. \quad (1)$$

Overall shrinkage of the specimens was generally low in both cases and lower for bi-S crosslinked samples compared to CE crosslinked samples (Table 3). Interestingly, the difference in volumetric shrinkage was very low for samples with 50 and 65 wt% crosslinker content. Most impressively, net-near-zero shrinkage of $\Delta V = -0.4\%$ was achieved for the 25% crosslinker-containing specimen based entirely on spiro-orthoester monomers.

Additionally, birefringence of optically transparent cured bulk samples impressively demonstrated how shrinkage stress at the edges is significantly reduced for samples with high spiro-orthoester monomer content (Fig. 5).

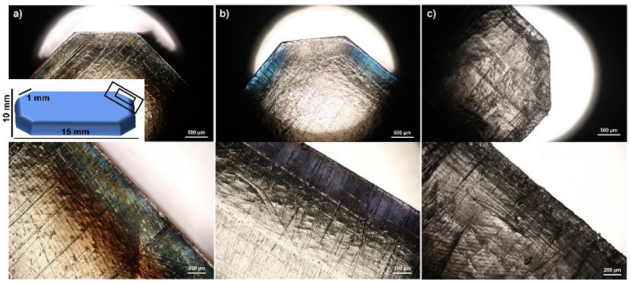

Fig. 5 Optical microscopy images of transparent bulk-cured samples for (a) 0, (b) 35 and (c) 75 wt% 5P-S content crosslinked with the diepoxide CE.

Table 3 Volumetric shrinkage in % for specimens containing 5P-S and different types (bi-S, CE) and amounts (25–75%) of crosslinkers

	Crosslinker type	
Crosslinker content/wt%	bi-S	CE
25	−0.4	−1.63
50	−2.4	−2.96
65	−2.2	−2.95

Hot lithography

Laser-exposure tests were performed to prove the printability of the optimized formulation containing the aromatic spiro-orthoester and the bifunctional epoxide. Since the formulation containing 65 wt% epoxide CE and 35 wt% 5P-S led to the best thermomechanical properties and exhibited the highest reactivity, the same monomer composition was used for laser-exposure tests on a Hot Lithography prototype setup with a 375 nm laser at 100 °C. In addition to the spiro-orthoester 5P-S (35 wt%) and the epoxide CE (65 wt%), the printing formulation contained the photoacid generator IC 290 (1 wt%) to initiate photopolymerization and the photosensitizer 9,10-dibutoxyanthracene (DBA, 0.1 wt%), which is used to absorb light at the printing light source wavelength (375 nm) and transfer the energy to the used photoinitiator (λ_{max} = 318 nm, Fig. S6B†).[35,36]

During the laser-exposure tests, diffusional overpolymerization was observed, which is a rather common phenomen in cationic photopolymerization.[37] It takes place when the formed superacid diffuses out of the irradiated area into the adjoining areas of the formulation. To eliminate overpolymerization, small amounts of ethyl-4-(dimethylamino)benzoate (EDAB) were added to the formulation to neutralize diffused acid. An optimized concentration of the base was determined as 0.1 wt% to maintain the reactivity of the system while hindering overpolymerization through diffusion.

For the final proof of concept, a four-sided pyramid was designed as CAD-file (diagonal section: 15 mm, side length: 10.6 mm) and the object was successfully printed *via* Hot Lithography at 100 °C (Fig. 6). The layer thickness was chosen to be 100 μm and the laser scan speed was set to 200 mm s^{-1}. The object exhibits clearly defined edges and layers without signs of overpolymerization. Good dimensional part accuracy compared to the CAD-model was achieved, with highly satisfying resolution and convincing surface finish. Good layer adhesion was additionally confirmed with scanning electron microscopy.

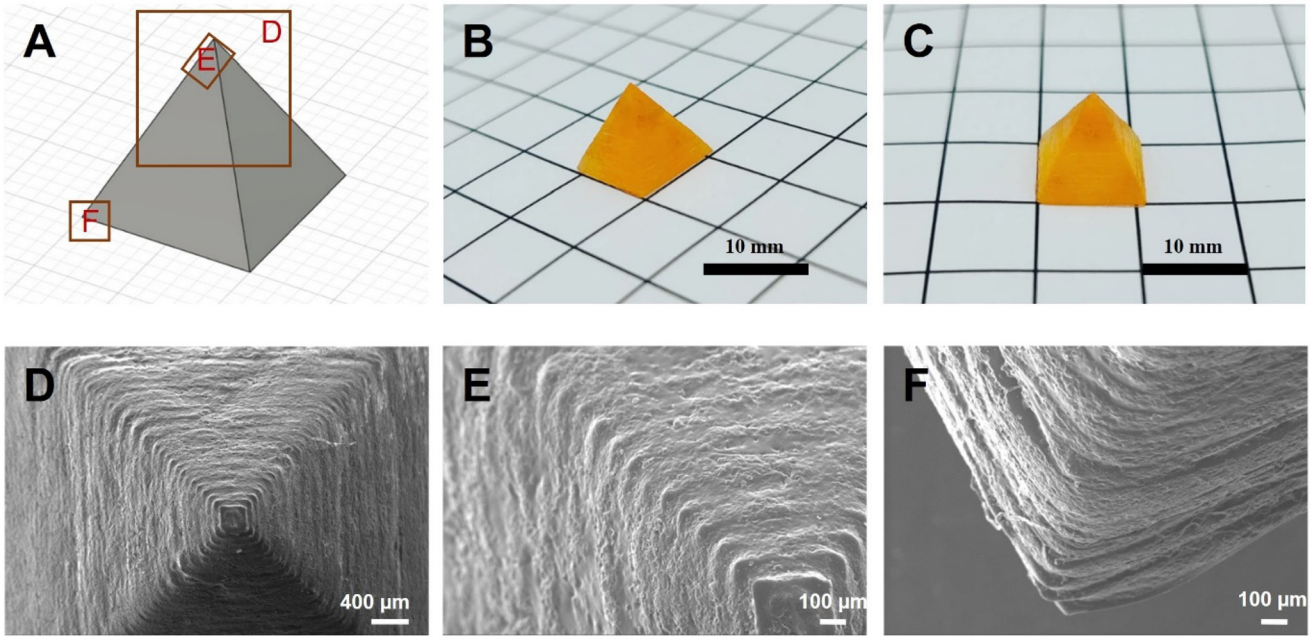

Fig. 6 Design of the printed pyramid (A), side-view of the printed part (B), front-view of the printed part (C), and SEM-images of the printed part as indicated in A (D–F).

Conclusions

Cationic polymerization of expanding spiro-orthoesters and their volume change upon polymerization is well-studied in literature. However, light-induced cationic polymerization of these highly interesting compounds and polymerization modes as a function of temperature have not been investigated in detail to date. Herein, the temperature-dependent light-induced cationic ROP of spiro-orthoesters with different ring sizes has been examined extensively. It was shown that the monomer ring-size and the polymerization temperature influence conversion, polymerization modes and molecular weights of the resulting polymers. The five-membered 5-S and 5P-S as well as the seven-membered 7-S were found to be suitable monomers for cationic photopolymerization due to their good reactivity and favourable polymerization mechanism. Based on these promising monomers, pure poly(ether–ester) networks have been developed using the spiro-orthoester crosslinker bi-S or an epoxide crosslinker. Biocompatible and biodegradable poly(ether–esters) were obtained by bulk-photopolymerization in both cases and tested (thermo-)mechanically. Finally, the spiro-orthoester/epoxide system was printed at 100 °C with high part-size accuracy and resolution. This SL process relies on pure cationic ring-opening polymerization without the need for a radical polymerization mechanism to accelerate curing, which allows for the production of pure polyether–ester networks *via* SL printing for the first time. The high part size precision and good thermomechanical properties as well as the biocompatibility and degradability of resulting parts open up a plethora of biomedical applications for the developed photoresist.

Author contributions

Danijela Kojic: investigation, methodology, validation, formal analysis, data curation, writing – original draft, writing – review & editing, visualization, project administration Katharina Ehrmann: supervision, conceptualization, methodology, formal analysis, data curation, writing – original draft, writing – review & editing, visualization, project administration Raffael Wolff: investigation, methodology, formal analysis Yazgan Mete: formal analysis, methodology, writing – review & editing, project administration Thomas Koch: methodology, formal analysis, data curation, writing – review & editing Jürgen Stampfl: methodology, writing – review & editing Stefan Baudis: formal analysis, funding acquisition, writing – review & editing Robert Liska: supervision, conceptualization, funding acquisition, methodology, formal analysis, writing – review & editing.

Conflicts of interest

There are no conflicts to declare.

References

1 S. C. Ligon, R. Liska, J. Stampfl, M. Gurr and R. Mülhaupt, Polymers for 3D Printing and Customized Additive Manufacturing, *Chem. Rev.*, 2017, **117**, 10212–10290.
2 A. Bagheri and J. Jin, Photopolymerization in 3D Printing, *ACS Appl. Polym. Mater.*, 2019, **1**, 593–611.

3 M. Pfaffinger, Hot Lithography – New Possibilities in Polymer 3D Printing, *Laser Tech. J.*, 2018, **15**, 45–47.
4 B. Steyrer, B. Busetti, G. Harakály, R. Liska and J. Stampfl, Hot Lithography vs. room temperature DLP 3D-printing of a dimethacrylate, *Addit. Manuf.*, 2018, **21**, 209–214.
5 J. Zhang and P. Xiao, 3D printing of photopolymers, *Polym. Chem.*, 2018, **9**, 1530–1540.
6 S. R. Schricker, in *Orthodontic Applications of Biomaterials*, ed. T. Eliades and W. A. Brantley, Woodhead Publishing, 2017, pp. 153–170, DOI: 10.1016/B978-0-08-100383-1.00009-6.
7 Y. Lochee, D. Jhurry, A. Bhaw-Luximon and A. Kalangos, Biodegradable poly(ester-ether)s: ring-opening polymerization of D,L-3-methyl-1,4-dioxan-2-one using various initiator systems, *Polym. Int.*, 2010, **59**, 1310–1318.
8 J. M. Pachence and J. Kohn, in *Principles of Tissue Engineering*, ed. R. P. Lanza, R. Langer and J. Vacanti, Academic Press, San Diego, 2nd edn, 2000, pp. 263–277, DOI: 10.1016/B978-012436630-5/50026-X.
9 R. Shi, D. Chen, Q. Liu, Y. Wu, X. Xu, L. Zhang and W. Tian, Recent Advances in Synthetic Bioelastomers, *Int. J. Mol. Sci.*, 2009, **10**, 4223–4256.
10 M. Okada, in *Polymer Synthesis Oxidation Processes*, Springer Berlin Heidelberg, Berlin, Heidelberg, 1992, pp. 1–46, DOI: 10.1007/3-540-55090-9_1.
11 M. L. R. K. Sadhir, *Expanding monomers: Synthesis, characterization, and applications*, 1992.
12 S. Chikaoka, T. Takata and T. Endo, Cationic ring-opening polymerization of spiroorthoester: polymer structure, polymerization mechanism, and volume change on polymerization, *Macromolecules*, 1992, **25**, 625.
13 P. Marx and F. Wiesbrock, Expanding Monomers as Anti-Shrinkage Additives, *Polymers*, 2021, **13**, 806.
14 S. Chikaoka, T. Takata and T. Endo, Copolymerization utilizing an equilibrium polymerization system: cationic copolymerizations of 1,4,6-trioxaspiro[4.6]undecane with 2-methyl-1,4,6-trioxaspiro[4.5]decane and 2-methyl-1,4,6-trioxaspiro[4.4]nonane, *Macromolecules*, 1991, **24**, 6563–6566.
15 S. Chikaoka, T. Takata and T. Endo, New aspects of cationic polymerization of spiroorthoester: cationic single ring-opening polymerization and equilibrium polymerization, *Macromolecules*, 1991, **24**, 6557–6562.
16 E. Klemm, Photoinduced spiro ortho ester-epoxide copolymerization, *Z. Anal.*, 1984, **24**(11), 412.
17 Y.-G. Hsu and Y.-S. Wan, Cationic Photopolymerization of cis-2,3-Tetramethylene-1,4,6-trioxaspiro[4,4]nonane, *J. Polym. Sci., Part A: Polym. Chem.*, 2009, **47**, 3680–3690.
18 P. Marx, A. Romano, R. Fischer, I. Roppolo, M. Sangermano and F. Wiesbrock, Dual-Cure Coatings: Spiroorthoesters as Volume-Controlling Additives in Thiol–Ene Reactions, *Macromol. Mater. Eng.*, 2019, **304**, 1800627.
19 M. Gagliardi and A. Bifone, Ring-opening copolymerization thermodynamics and kinetics of γ-valerolactone/ε-caprolactone, *PLoS One*, 2018, **13**, e0199231.
20 P. Olsén, K. Odelius and A.-C. Albertsson, Thermodynamic Presynthetic Considerations for Ring-Opening Polymerization, *Biomacromolecules*, 2016, **17**, 699–709.
21 K. Bodenbenner, Über spirocyclische Orthoester, *Justus Liebigs Ann. Chem.*, 1959, **623**, 183–190.
22 H. Nishida, F. Sanda, T. Endo, T. Nakahara, T. Ogata and K. Kusumoto, Addition reaction of spiro orthoesters with electrophiles: A model reaction for the development of novel polyaddition accompanying ring-opening isomerization, *J. Polym. Sci., Part A: Polym. Chem.*, 1999, **37**, 4502–4509.
23 W. Bailey, H. Iwama and R. Tsushima, Synthesis of elastomers by cationic polymerization with expansion in volume, *J. Polym. Sci., Polym. Symp.*, 2007, **56**, 117–127.
24 A. Vitale, M. Sangermano, R. Bongiovanni, P. Burtscher and N. Moszner, Visible Light Curable Restorative Composites for Dental Applications Based on Epoxy Monomer, *Materials*, 2014, **7**, 554–562.
25 N. Guy, O. Giani, S. Blanquer, J. Pinaud and J.-J. Robin, Photoinduced ring-opening polymerizations, *Prog. Org. Coat.*, 2021, **153**, 106159.
26 C. J. Martin, G. Rapenne, T. Nakashima and T. Kawai, Recent progress in development of photoacid generators, *J. Photochem. Photobiol. C: Photochem. Rev.*, 2018, **34**, 41–51.
27 S. Penczek, J. Pretula and S. Slomkowski, Ring-opening polymerization, *Chem. Teach. Int.*, 2021, **3**, 33–57.
28 A. Duda and A. Kowalski, in *Handbook of Ring–Opening Polymerization*, 2009, pp. 1–51, DOI: 10.1002/9783527628407.ch1.
29 T. Takata and T. Endo, Recent advances in the development of expanding monomers: Synthesis, polymerization and volume change, *Prog. Polym. Sci.*, 1993, **18**, 839–870.
30 Y.-G. Hsu, Y.-S. Wan, W.-Y. Lin and W.-L. Hsieh, Cationic Polymerization of cis-2,3-Tetramethylene-1,4,6-trioxaspiro[4,4]nonane Photosensitized by Anthracene, *Macromolecules*, 2010, **43**, 8430–8435.
31 Y.-G. Hsu, W.-Y. Lin, W.-L. Hsieh and S.-Y. Tsai, Regiospecific cationic polymerization of spiroorthoesters with different cyclic ether ring sizes, *J. Polym. Sci. A Polym. Chem.*, 2012, **50**, 720–728.
32 Y.-G. Hsu, W.-Y. Lin, W.-L. Hsieh and S.-Y. Tsai, Regiospecific cationic polymerization of spiroorthoesters with different cyclic ether ring sizes, *J. Polym. Sci., Part A: Polym. Chem.*, 2012, **50**, 720–728.
33 J. Canadell, A. Mantecón and V. Cádiz, Crosslinking of a polyacrylate bearing a spiroorthoester pendant group with mixtures of diglycidyl ether of bisphenol A and phosphorus-containing glycidyl derivatives, *J. Polym. Sci., Part A: Polym. Chem.*, 2007, **45**, 1920–1930.
34 J. Canadell, A. Mantecón and V. Cádiz, Synthesis of a novel bis-spiroorthoester containing 9,10-dihydro-9-oxa-10-phosphaphenantrene-10-oxide as a substituent: Homopolymerization and copolymerization with diglycidyl ether of bisphenol A, *J. Polym. Sci., Part A: Polym. Chem.*, 2007, **45**, 1980–1992.
35 J. V. Crivello and M. Jang, Anthracene electron-transfer photosensitizers for onium salt induced cationic photopo-

lymerizations, *J. Photochem. Photobiol., A*, 2003, **159**, 173–188.
36 N. Klikovits, P. Knaack, D. Bomze, I. Krossing and R. Liska, Novel photoacid generators for cationic photopolymerization, *Polym. Chem.*, 2017, **8**, 4414–4421.
37 N. Klikovits, L. Sinawehl, P. Knaack, T. Koch, J. Stampfl, C. Gorsche and R. Liska, UV-Induced Cationic Ring-Opening Polymerization of 2-Oxazolines for Hot Lithography, *ACS Macro Lett.*, 2020, **9**, 546–551.